Inorganic Chemistry

pubs.acs.org/IC

Article

Osmium(III) Acetylacetonate and Its Missing Polymorph: A Magnetic and Structural Investigation

Arsen Raza, Laura Chelazzi, Samuele Ciattini, Lorenzo Sorace, and Mauro Perfetti*

Cite This: *Inorg. Chem.* 2024, 63, 17198−17207

Read Online

ACCESS | Metrics & More | Article Recommendations | Supporting Information

ABSTRACT: Despite the potential for their application, the magnetic behavior of complexes containing 4d and 5d metal ions is underexplored, evidencing the need for benchmark multi-technique studies on simple molecules. We report here a structural and magnetic study on osmium(III) acetylacetonate $[Os(acac)_3]$. X-ray single crystal diffraction did not allow us to determine the structure of the β-polymorph of $[Os(acac)_3]$. The combined magnetic (dc magnetic measurements on powder and cantilever torque magnetometry on single crystal) and spectroscopic (electron paramagnetic resonance, EPR) characterization is here used to provide further evidence that its structure is indeed the one of the orthorhombic "missing polymorph", analogous to the ruthenium(III) derivative. Our study shows that all acetylacetonate complexes of the eighth group of the periodic table show dimorphism and are isomorphic. The EPR characterization allowed the experimental assessment of the easy axis nature of the ground doublet and the determination of the first hyperfine coupling in an osmium complex. Torque magnetometry, applied here for the first time on an osmium-based molecule, determined the orientation of the easy axis along the pseudo C_3 axis of the complex. Ac magnetometric measurements revealed in-field slow relaxation of the magnetization further slowed by the suppression of dipolar fields via magnetic dilution in the isostructural gallium(III) analogue.

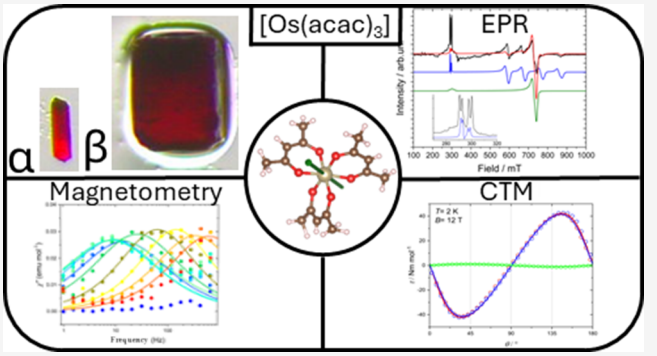

1. INTRODUCTION

Since their first discovery, transition metal complexes have been studied for their fascinating magnetic behavior. Careful engineering of the ligand field and the magnetic anisotropy of the metal complex has also given momentum to the research on single molecule magnets (SMM) based on single metal centers.[1] Complexes containing light transition metals are nowadays vastly investigated as molecular qubits with remarkable performances.[2−6] Moving toward heavy atoms, the metal complexes tend to exhibit low spin configurations, often leading to diamagnetic molecules. At the same time, the enhanced radial extension of the valence orbitals and the large values of the spin−orbit constant constitute in principle an ideal resource to promote strong magnetic interactions and/or to create highly anisotropic building blocks.[7−13]

However, the stabilization of specific oxidation states poses significant synthetic challenges. Moreover, the large spin-orbit coupling imposes taking into account the (partially) unquenched orbital angular momentum, rendering the standard spin Hamiltonian treatment inadequate. This makes the magnetic behavior of heavy transition metal complexes underexplored, resulting in a poor exploitation of the properties of species containing 4d and 5d metals. Therefore, benchmark multi-technique studies on simple complexes bearing heavy transition metals are much needed. We decided to focus our attention on a surprisingly poorly studied complex of a 5d ion: osmium(III) acetylacetonate, $[Os(acac)_3]$.

The first structure of a transition metal complex with acetylacetone as a sole ligand in the general formula $[M(acac)_n]$ (Hacac = acetylacetone; n = 1, 2, 3 or 4) archived in the Cambridge Structural Database (CSD)[14] dates back to 1926 and it refers to $[Sc(acac)_3]$.[15] Since then, the chemistry of these simple molecules has been heavily explored for a number of applications.[16,17] Acetylacetones are chemically simple and tunable ligands, prone to structural modifications by replacing their α-hydrogen atoms or the methyl groups with other fragments. Such chemical flexibility allows the fine-tuning of several properties such as solubility, volatility, color, and melting point of the resultant metal complexes.[18−20] At present, they are used as starting materials for the synthesis of nanoparticles,[21] they have a relevant role in polymeric production processes,[22−24] and are used as catalysts precursors in many organic syntheses.[25−29] The most characterized and studied complexes

Received: April 24, 2024
Revised: June 22, 2024
Accepted: July 29, 2024
Published: August 2, 2024

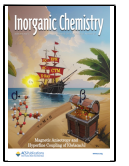

contain 3d metals,[30−37] even though some examples are reported also for the second transition series.[38,39] For 5d elements there are only a few examples in the literature.[40−43]

Figure 1 shows the crystal system in which the various transition metal complexes crystallize. The monoclinic system

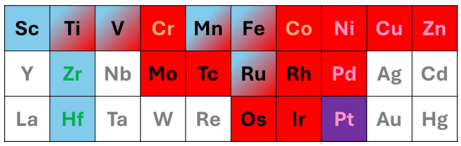

Figure 1. Pictographic representation of the different structures reported for generic homoleptic complexes of the formula $[M(acac)_n]$, where M = transition metal. Color code of background: Red = monoclinic, Blue = orthorhombic, Violet = triclinic. Color code of oxidation state of the metal: pink = +2, black = +3, green = +4, orange = +2 and +3, and gray = N/A.

predominates with a space group number of 14 ($P2_1/n$ or $P2_1/c$). However, neutral species with the generic formula $[M(acac)_3]$ often exhibit polymorphism. Indeed, several complexes reported as monoclinic also crystallize in the *Pbca* orthorhombic space group. Examples are the complexes of titanium(III),[16,44] vanadium(III),[45−47] manganese(III),[16,48,49] and iron(III).[16,50] Following the recent literature,[16] we will hereafter label the monoclinic form as α-polymorph and the orthorhombic form as β-polymorph. For the second and third transition periods, the only reported polymorphic species is $[Ru(acac)_3]$.[51,52] Therefore, Group 8 of the periodic table is the only one where two elements present bimorphism, with the "missing polymorph" being the *Pbca* orthorhombic form of the $[Os(acac)_3]$ complex.

$[Os(acac)_3]$ is an excellent starting material for synthetic pathways requiring osmium in the +3 oxidation state, such as the synthesis of nanoparticles[53] and SMM.[54] Recently, $[Os(acac)_3]$ has also aroused interest because it has been predicted to be an excellent candidate to observe molecular parity violation phenomena.[55]

In this study, we demonstrate that the polymorphism observed for $[Fe(acac)_3]$ and $[Ru(acac)_3]$ is also occurring for $[Os(acac)_3]$. A detailed single-crystal cantilever torque magnetometry (CTM) study delivered the main magnetic anisotropy axes and provided unequivocal evidence that the second polymorph is isostructural with the Ruthenium analogue. Moreover, we used electron paramagnetic resonance (EPR) spectroscopy, dc and ac magnetometry to characterize the electronic structure, and the static and dynamic magnetic behavior of the complex, rationalizing all the experimental observations by using a simple ligand-field based model.

2. EXPERIMENTAL SECTION

2.1. General Methods and Materials. *2.1.1. General Procedures.* The synthesis was performed by excluding oxygen by using normal Schlenk procedures. Once the complex is formed, the exclusion of air is no longer necessary. All the solvents, the precursor, and the compounds used in the synthesis are commercially available and were used without further purification. IR spectra were recorded with a PerkinElmer FT-IR 100 instrument. UV−vis spectra were recorded on a Jasco V-670 double-beam spectrophotometer by using quartz cuvettes of 1 cm length.

2.1.2. Synthesis of Osmium Acetylacetonate(III) - [Os(acac)$_3$]. In a double-neck flask with a stir bar, under N_2, Ag^0 flakes (400.7 mg, 3.714 mmol) and $(NH_4)_2OsCl_6$ (204.0 mg, 0.4647 mmol) are placed. In another single-neck flask, deionized water (10 mL) and 1 mL of concentrated HBr are added, and then N_2 is bubbled for 30 min. The acidic solution is cannulated in the double-neck flask, and N_2 is bubbled for 12 h. The suspension became orange yellow; 1.50 g of $KHCO_3$ and 2 mL of acetylacetone were added. The suspension is refluxed for 20 min, and then 1.2 g of $KHCO_3$ and 5 mL of acetylacetone are added again. The suspension, after being refluxed for 2 h, becomes brown-purple. The suspension is left to cool and subsequently extracted with $CHCl_3$ (10 mL × 6) and all the fractions are collected together in a single brown solution which is washed with 2% NaOH solution. The solvent is removed under vacuum, and 108.5 mg (47.89% yield) of brown powder is obtained. ATTENTION: elemental analysis of osmium complexes cannot be performed for safety reasons since the combustion produces OsO_4, a volatile and extremely toxic compound. IR-ATR (cm^{-1}): 1531 (s), 1512 (s), 1506 (s) 1418 (m), 1372 (s), 1353 (s), 1274 (s), 1198 (m), 1023 (m), 1009(m), 938 (m), 809 (w), 777 (m), 688 (w), 659 (l), 632 (s), 458 (s), 429 (m). UV−Vis−NIR (acetonitrile, $c = 5.0 \times 10^{-5}$ M): λ max (ε) = 203 nm (9.9×10^3 M^{-1} cm^{-1}); 235 nm (9.8×10^3 M^{-1} cm^{-1}); 266 nm (22.5×10^3 M^{-1} cm^{-1}), ∼ 311 nm (∼4.1×10^3 M^{-1} cm^{-1}); 368 nm (10.2×10^3 M^{-1} cm^{-1}) ∼ 419 nm (∼4.7×10^3 M^{-1} cm^{-1}). Crystallization from H_2O/EtOH (1:1) provided both polymorphs based on PXRD. Crystallization by slow evaporation of $CHCl_3$ selectively produced the β form.

2.1.3. Synthesis of 2% [Os(acac)$_3$] in [Ga(acac)$_3$] (Os@[Ga(acac)$_3$]). An amount of 4.0 mg of $[Os(acac)_3]$ and 196.0 mg of $[Ga(acac)_3]$ are solubilized in 70 mL of $CHCl_3$. The solution is left to evaporate and a microcrystalline solid is obtained (Figure S2 Supporting Information).

2.1.4. X-ray Crystallography. Single-crystal X-ray diffraction data were collected at 100 K using a Bruker D8 Venture diffractometer equipped with a PHOTON II detector and a microfocus source (Cu Kα radiation, λ = 1.54184 Å). Data were corrected for absorption effects using the multiscan method (SADABS). The crystal structure was solved and refined using the Bruker SHELXTL. For the Single-crystal X-ray diffraction measurement at 15 K, an Oxford Diffraction Xcalibur3 CCD four-circle diffractometer with a graphite monochromator and Mo-Ka radiation, equipped with an Helijet cryostat, was used. The data set was corrected for Lorentz and polarization effects, and absorption corrections were performed by the ABSPACK multiscan procedure of the CrysAlis (CrysAlis RED, n.d., version 171.37.35) data reduction package. The structure was solved using the direct method with the SIR-2019 software, and refinement was performed using the SHELXL-2013[56] included in the Wingx software package.[57]

Powder X-ray diffraction (PXRD) patterns were recorded on a Bruker New D8 Advance DAVINCI diffractometer in a theta−theta configuration equipped with a linear detector. Crystalline powders were mounted on a zero-background diffraction plate. The scans were collected within the range 5°−50° (2θ), using Cu Kα radiation. For the Pawley fit with the software TOPAS, a shifted Chebyshev polynomial with 5 coefficients and a pseudo-Voigt function were used to fit the background and peak shape, respectively (see Figures S1 and S2 in the Supporting Information). The unit-cell parameters and the Rwp factor for the powder pattern are calculated and reported in Tables S1 and S2 of the Supporting Information.

2.1.5. Magnetic Measurements. A Quantum Design Magnetic Properties Measurement magnetometer equipped with a Superconducting Quantum Interference Device Direct was used to perform the dc and ac magnetic characterization. Temperature- and field-dependent dc magnetization measurements were performed in the 2.0−300 K temperature range on a β-$[Os(acac)_3]$ sample (26.22 mg) wrapped in Teflon and pressed in pellet, with an applied magnetic field of 0.1 T and at temperatures between 2 and 10 K with applied field up to 5 T. The measured magnetic moment has been corrected for a diamagnetic contribution of -2.7×10^{-6} emu to account for the diamagnetism of Teflon and straw; the molar paramagnetic susceptibility of the complex has been obtained by further considering the intrinsic diamagnetic contribution of the molecule (-192×10^{-6} emu/mol, evaluated by Pascal's constants[58]). No correction was applied for temperature independent paramagnetism (TIP). Experimental results were modeled using the *curry* function of Easyspin.[59] Ac susceptibility measurements were performed on pellets of both β-$[Os(acac)_3]$ and on Os@$[Ga(acac)_3]$, with a frequency range from 1 to

https://doi.org/10.1021/acs.inorgchem.4c01672
Inorg. Chem. 2024, 63, 17198−17207

1000 Hz at 2 K. Ac susceptibility data were fitted using a home developed program.[60]

2.1.6. EPR Spectroscopy. X-band ($\nu \cong 9.40$ GHz) CW-EPR spectra were recorded on a Bruker Elexsys E500 spectrometer equipped with an ER4122SHQE resonator. Low temperature measurements (5 K) were obtained using an Oxford Instruments ESR900 continuous flow helium cryostat and temperature controlled by an Oxford Instruments ITC503. The spectrum of Os@[Ga(acac)$_3$] was simulated with Easyspin[59] (see the Supporting Information for further details).

2.1.7. Torque Magnetometry. The cantilever torque measurements were performed using a homemade two-leg CuBe cantilever separated by 0.1 mm from a gold plate. The cantilever was inserted in an Oxford Instruments MAGLAB2000 platform with automated rotation of the cantilever chip into a vertical magnet. The capacitance of the cantilever was detected with an Andeen-Hegerling 2500A Ultra Precision Capacitance Bridge. The torque measurements were simulated using a home-written program partially based on EasySpin.[59]

3. RESULTS AND DISCUSSION

3.1. Synthesis and Structural Characterization. The first synthesis of [Os(acac)$_3$] was reported in 1955.[61] In this procedure, Dwyer and Sangerson used silver wool in the presence of HBr to reduce the level of ligand in $OsBr_6^{2-}$ and subsequently a great excess of ligand was added. The product was extracted in organic solvents and recrystallized even though no structural information was provided. In 1998 Dallmann and Preetz[40] reported the first structure of [Os(acac)$_3$]. In their paper an Osmium(IV) salt was used as the starting material, but the absence of a reducing agent resulted in a negligible yield (5%). Our attempts to repeat this reaction did not show any trace of product formation; therefore, we attribute the nonzero yield of their synthesis to the presence of reducing impurities.

We have reproduced the procedure used by Dwyer and Sangerson with a slight modification,*i.e.*, by using silver flakes instead of silver wool. This procedure significantly reduces the costs and provides comparable yield (48%). We isolated two morphologically different crystalline forms of [Os(acac)$_3$], rectangular and elongated prisms (see Figure S3 in the Supporting Information), both intensely red colored. Single-crystal X-ray diffractometry measurements at 100 K on the elongated prism shaped crystals demonstrated that they belong to the $P2_1/c$ monoclinic form reported by Dallmann and Preetz, isostructural with the α-polymorph of [Ru(acac)$_3$]. On the contrary, the structure of the rectangular prisms could not be solved. Indeed, the indexing of cell parameters with several crystalline systems gave reasonable starting points for the solution but inevitably ended with the same problem in resolution: namely, the position of the heavy metal center and of the coordinating oxygen atoms could be easily identified, but it was impossible to reliably define the ligand structure. In order to reduce the thermal disorder of the ligands, we performed a single crystal X-ray measurement at very low temperature (15 K), but also in this case, the assignment of the position of the light atoms that constitute the structure of the ligand failed.

The difficulties in resolving the structure of small molecules containing heavy atoms are well-known in the literature.[62] Giacovazzo introduced the empirical parameter $P = \sum_{h=1}^{n} Z_h^2 / \sum_{l=1}^{m} Z_l^2$ (where Z_h and Z_l are the atomic numbers of heavy and light atoms, respectively, and summations run over the n and m heavy and light atoms, respectively) to estimate the difficulty of structural refinement. P values higher than 2 correspond to an easy solution but a bad accuracy in defining the position of lights atoms in the structure.[63] The P value for [Os(acac)$_3$] is 6.11, suggesting a possible difficulty in determining the positions of the light atoms in this structure. However, since the same value for this parameter is obtained for the first polymorph, we speculate that other factors may contribute in making the structural solution impossible. Among these, the difficulty in obtaining an effective absorption correction due to the fairly anisotropic crystal morphology (see Supporting Information), and the possible presence of pseudo symmetry effects.

To partially overcome this issue, we collected a powder X-ray diffractogram on a sample constituted by crushed rectangular prismatic crystals (Figure S1 in the Supporting Information). Interestingly, this could be fitted using the Pawley method as implemented in the Topas software[64,65] by using cell parameters close to the ones of the β-polymorphs of [Ru(acac)$_3$] and [Fe(acac)$_3$] (Table S1 of the Supporting Information), suggesting isomorphism with these two derivatives.

3.2. CW-EPR. Since crystallography did not give conclusive results on the structure and symmetry of the rectangular prismatic crystals, we decided to combine two powerful techniques that can relate the magnetic properties of metal complexes with their structure, namely, EPR and CTM. EPR is very sensitive to the principal values of the $\boldsymbol{g}$ factor of the metal ion, while CTM allows a precise determination of the direction of the magnetic anisotropy axes of the molecule.

Examples of CW-EPR investigation on osmium(III) complexes are rare,[66−69] but they clearly identify these molecules as low spin d^5 complexes ($S = 1/2$) with residual orbital angular momentum, due to the $^2T_{2g}$ nature of its ground state in octahedral symmetry. X-Band CW-EPR on a microcrystalline powder of prismatic rectangular [Os(acac)$_3$] crystals did not show any signal down to 5 K, probably due to fast relaxation induced by spin−spin interactions. We were also unable to observe any EPR spectrum of [Os(acac)$_3$] in toluene solution as low as 5 K. Therefore, we prepared a solid solution of 2% [Os(acac)$_3$] in the diamagnetic [Ga(acac)$_3$] (Os@[Ga(acac)$_3$]). The resultant powder is a mixture of α- and β-polymorphs (ca. 75:25, as obtained by PXRD, See Figure S2 in Supporting Information) but at low temperature (Figure 2) provides an EPR spectrum which can be assigned to a single species, as expected from the chemical similarity (same angles and distances) observed for the structure of the two polymorphs of [Ru(acac)$_3$]. The observed spectrum can be qualitatively interpreted as arising from a spin doublet with $g_{\parallel} > 2.00 > g_{\perp}$ and a fraction of the electronic spins being hyperfine coupled to an active nuclear spin, as expected for Osmium (^{189}Os, n.ab.= 16.15%, $I = 3/2$; ^{187}Os, n.ab.= 1.96%, $I = 1/2$, the remaining isotopes are nuclear spin free). Following this interpretation, we attempted a simulation of the spectrum by using a Hamiltonian containing an anisotropic Zeeman term and hyperfine coupling term for the fraction of molecules containing a nonzero nuclear spin:

$$\hat{H}_s = \mu_B \mathbf{B}\cdot\mathbf{g}\cdot\hat{S} + \hat{S}\cdot\mathbf{A}^{Os}\cdot\hat{I}^{Os} \quad (1)$$

We could obtain a reasonable simulation by using $g_x = 0.925 \pm 0.002$, $g_y = 0.905 \pm 0.002$, $g_z = 2.2271 \pm 0.002$, $|A_{x,y}| = 1170 \pm 10$ MHz and $|A_z| = 18 \pm 2$ MHz, where the small rhombicity of the $\boldsymbol{g}$ tensor is needed to reproduce the partial split of the perpendicular line of the $I = 0$ isotope close to 720 mT. It is worth noting that by using this set of parameters, and assuming a narrower parallel line width for the contribution of [^{189}Os(acac)$_3$] than for the $I = 0$ ones, we were able to obtain the peculiar unequally spaced four lines pattern observed around

https://doi.org/10.1021/acs.inorgchem.4c01672
Inorg. Chem. 2024, 63, 17198−17207

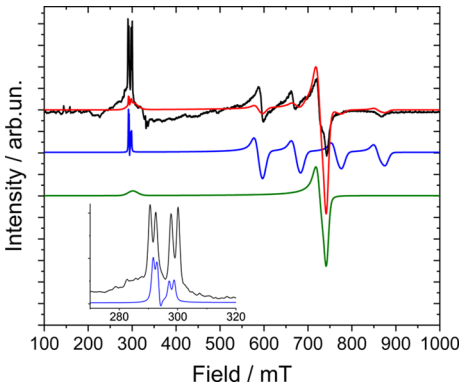

Figure 2. Experimental (black) and simulated (red, blue, and green) X-band (9.397 GHz) CW-EPR spectra of Os@[Ga(acac)$_3$] at T = 5 K. The best simulation parameters are reported in the main text. Simulation of the two main contributions to the spectra of [Os(acac)$_3$] and their combination according to natural abundance is given. Blue: spectrum of ^{189}Os (I = 3/2, nat. ab.= 16.15%); Green: spectrum of the I = 0 isotopes of osmium (total nat. ab. = 81.89%). The contribution of ^{187}Os (I = 1/2, nat. ab. = 1.96%) is not visible in the experimental spectrum and is not reported here. Red: sum of blue and green traces. The inset reports a zoomed-in view of the experimental $g_{\|}$ region to evidence the superimposed "doublet of doublets" structure with the simulation of the ^{189}Os contribution only (blue trace).

290 mT (see inset of Figure 2). The origin of this specific pattern lies in the large and very anisotropic hyperfine coupling of this complex, for which the perpendicular component is much larger than the parallel component (Figure S4). As discussed by Chicco and co-workers, this results in an "effective" quadrupolar coupling,[70] which measurably splits the parallel lines even when A_z = 0 (see Figures S5 and S6 in the Supporting Information). Interestingly, the effect of this second-order effect on the parallel resonant fields is much stronger than that produced by any reasonable assumption on the magnitude of the real quadrupolar term expected for the I = 3/2 of ^{189}Os (see Figure S7 in the Supporting Information), which we then leave undetermined.

While still providing a simulated spectrum which is not perfect in terms of the relative intensity of different regions, our simulation captures the main features of the experimental spectrum: (i) the presence of 4 narrow and unequally spaced lines in the parallel region, superimposed on the broader transition due to the molecules with nonmagnetic transition metal nuclei; (ii) the presence of 4 almost equally spaced lines in the perpendicular region, centered around the line attributed to the $\underline{I}$ = 0 molecule (See Figure 2); (iii) a split of the lines in the perpendicular region which is consistent with the value of the perpendicular component of the hyperfine coupling providing the correct observed splitting in the parallel region.

To the best of our knowledge, this is the first hyperfine coupling resolved in an EPR spectrum of an osmium complex. We further notice that the obtained Spin Hamiltonian parameters are in good agreement with the few ones reported in the literature for osmium(III) complexes.[66−69,71] The close to axial g tensor reflects the dominant trigonal distortion from the perfect octahedral symmetry, typical of the tris-chelate structure around the metal center.[69,72,73] Moreover, the obtained anisotropy mirrors the conformational degrees of freedom of the ligand and the nature of the donor atoms. Indeed, the anisotropy that we recorded ($\Delta g = g_{\|} - g_{\perp} = 1.3121$) is intermediate between the one imposed by the loose monodentate ligands such as carbon monoxide, pyridine, cyanide, and the halide anions ($0.3 < \Delta g < 1$)[68,74] and the rigid bidentate ligands such as phenanthroline and bipyridine ($|\Delta g| \approx 2$),[69,71] but it is much larger than the one reported for Sulfur-based similar ligands such as [Os(sacsac)$_3$] (sacsac$^-$ = dithioacetylacetonate, Δg = 0.313).[67]

3.3. CTM. CTM is an extremely powerful technique for extracting information about magnetic anisotropy and can be performed on different type of samples[75] but is mostly utilized on single crystals.[76−78]

In the low-field, high-temperature limit the magnetic torque of a paramagnet can be expressed as follows:

$$\tau = \boldsymbol{M} \times \boldsymbol{B} = \Delta\chi \cdot B^2 \cdot \cos\varphi \sin\varphi \qquad (2)$$

where $\boldsymbol{M}$ is the magnetization of the sample, $\boldsymbol{B}$ is the magnetic field, $\Delta\chi$ is the anisotropy of the magnetic susceptibility in the scanned plane and φ is the angle between $\boldsymbol{M}$ and $\boldsymbol{B}$. Therefore, when an anisotropic paramagnet is rotated in a homogeneous magnetic field, the torque usually vanishes every 90° (*i.e.*, whenever the projection of the main magnetic axis of the sample in the scanned plane is parallel or perpendicular to the applied field). In the high-field, low-temperature limit, the shape of the

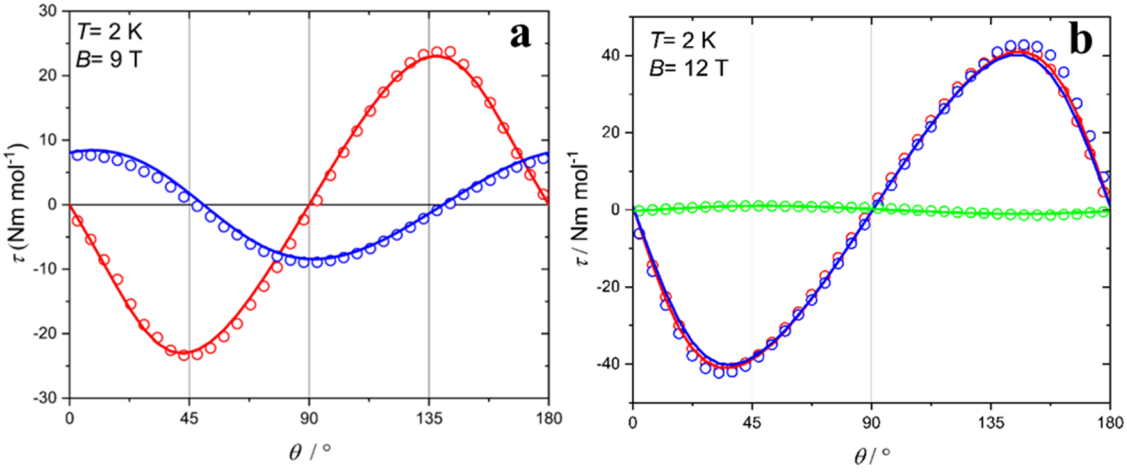

Figure 3. (a) Rot 1 (red) and Rot 2 (blue) for the α-polymorph. (b) Rot 1 (red), Rot 2 (blue), and Rot 3 (green) for the β-polymorph. The lines represent the best fit or simulation discussed in the main text.

https://doi.org/10.1021/acs.inorgchem.4c01672
Inorg. Chem. 2024, 63, 17198−17207

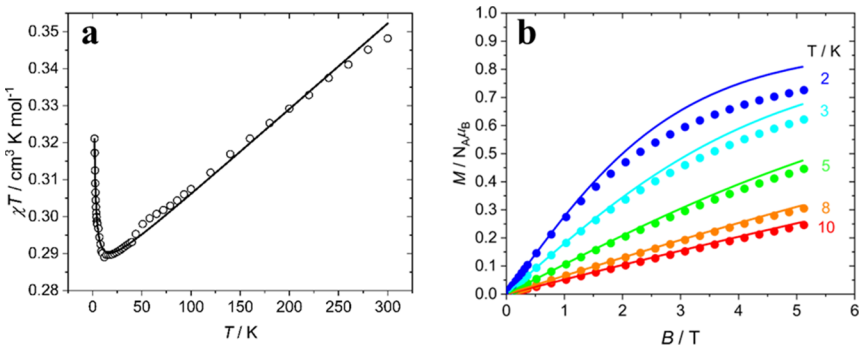

Figure 4. (a) Temperature dependence of the χT product of $[Os(acac)_3]$ recorded at H = 1 kOe; (b) Field dependent magnetization measured at different temperatures; For both panels, continuous lines were obtained using the model and best fit parameters reported in the text.

curve becomes more complicated, but the zero-torque angles maintain their significance.

To obtain some information about the magnetic anisotropy of the $[Os(acac)_3]$ molecule, we first studied the α-polymorph, for which we determined the crystal structure. Due to the presence of an inversion center and a C_2 axis in the unit cell, two magnetically inequivalent molecules are present. In the first rotation (Rot 1), performed around $-a$ starting with the field along $-c$, the zero torque signals observed at $\theta = 0°$ and $\theta = 90°$ are consistent with the C_2 axis along b. The second rotation (Rot 2) was performed around $-b$ and the magnetic field was positioned along c at $\theta = 0°$ (Figure S8 in the Supporting Information). Given the crystal symmetry, the projections of the easy axis of the two molecules in the scanned plane are now identical, producing zeros at $\theta = 48°$ (projection perpendicular to $\boldsymbol{B}$) and $\theta = 48° + 90° = 138°$ (projection parallel to $\boldsymbol{B}$).

The experimental torque curves (Figure 3) were fitted by using Hamiltonian (1) without including hyperfine interactions and by fixing the principal values of the substantially axial $\boldsymbol{g}$ tensor to the ones determined by CW-EPR (for $g_\perp$ the average $(g_x + g_y)/2 = 0.915$ was used), leaving the orientation of the easy axis as the only free parameter. Given the monoclinic nature of the investigated crystal, the best fit produced two equally good solutions (Figure S9 in the Supporting Information).[79] In the first one, the easy axis is lying almost along the ideal axis connecting two oxygen atoms of two different ligands; in the second one, it is almost parallel to the ideal C_3 axis of the molecule. This last solution is the one expected from symmetry considerations and coincides with the one previously reported for other $[M(acac)_3]$ complexes.[72,73]

Having rationalized the observed results for the α-polymorph, we moved to a CTM study of the rectangular crystals. Following the X-ray powder diffractogram, we indexed the crystal faces assuming the *Pbca* space group and we used as a reference the structure of the β-polymorph of $[Ru(acac)_3]$, the cell of which contains 4 magnetically inequivalent molecules. We performed three orthogonal rotations along the principal symmetry axes of the crystal (Rot 1, Rot 2 and Rot 3 along b, $-c$ and $-a$, respectively). The magnetic field at $\theta = 0°$ was along $-c$, $-b$, and $-b$, respectively. First, we notice that the torque always vanished at $\theta = 0°$ and $\theta = 90°$, *i.e.*, when the magnetic field is along a principal axis of the orthorhombic crystal. This is a direct experimental proof that the crystal structure has indeed orthorhombic symmetry. Moreover, we can observe that the torque signal is of comparable magnitude for Rot 1 and Rot 2, while it is significantly weaker for Rot 3 (1:40 compared to the other rotations). This immediately indicates that the easy axis orientation of the β-polymorph of $[Os(acac)_3]$ has a very small projection in the plane scanned in Rot 3 and should then lie close to the crystallographic a axis (*i.e.*, the rotation axis of Rot 3). Interestingly, an inspection of the structure of the $[Ru(acac)_3]$ β-polymorph shows that the pseudo-C_3 axis of the molecules (corresponding to one of the two solutions identified in the α polymorph) is quite close to the a axis. We thus simulated the torque of the rectangular crystals by using the principal g values experimentally determined from EPR and the easy axis orientation obtained from CTM (*i.e.*, along the pseudo-C_3 axis). The simulation, with no adjustable parameters, reproduces the data perfectly (Figure 3b), demonstrating that we indeed isolated the orthorhombic *Pbca* polymorph of $[Os(acac)_3]$, isostructural with the $[Ru(acac)_3]$, and $[Fe(acac)_3]$ analogues.

3.4. Magnetometry. To complete the characterization, we performed a bulk magnetic characterization on the powder of the β-polymorph.

The value of χT of $[Os(acac)_3]$ at room temperature reaches 0.348 $cm^3\ K\ mol^{-1}$ (Figure 4a), confirming the low spin nature of the complex.[40] Upon lowering the temperature, χT drops almost linearly to 0.289 $cm^3\ K\ mol^{-1}$ and then rises again below 12 K, reaching 0.321 $cm^3\ K\ mol^{-1}$ at 2 K. This shape is typical of systems with high spin−orbit coupling constants and low symmetry distortions in the presence of an overall ferromagnetic mean field. The magnetization curves do not saturate even at T = 2 K and B = 5 T, with the highest value (0.73 μ_B) being lower than the expected value for a spin of $S = 1/2$ with quenched orbital angular momentum. This indicates the presence of residual orbital angular momentum opposing the spin, as expected for heavy transition metals, even though this point is often misunderstood in the literature, generating confusion.[80]

In ideal octahedral symmetry the ground state of $[Os(acac)_3]$ is $^2T_{2g}$.[81] This six-fold degenerate state is split by first-order spin−orbit coupling in a low-lying doublet (formally $J = 1/2$) and a quadruplet (formally $J = 3/2$) by exploiting the T−P isomorphism.[81] The axial distortion from purely octahedral symmetry further separates the upper multiplet into two doublets (see Figure 5). The magnetic data were then fitted by using the following ligand field Hamiltonian:

$$\hat{H} = -3/2\kappa\lambda\hat{\mathbf{L}}\cdot\hat{\mathbf{S}} + 9/4\kappa^2 C_2^0\hat{\mathbf{O}}_2^0 + g_e\mu_B\mathbf{B}\cdot\hat{\mathbf{S}} - 3/2\kappa g_L\mu_B\mathbf{B}\cdot\hat{\mathbf{L}} \quad (3)$$

where the first term represents the spin−orbit coupling between the $S = 1/2$ and the $L_{eff} = 1$ angular momenta, the second term describes the axial component of the ligand field acting on the orbital angular momentum $L_{eff} = 1$ (with $\hat{\mathbf{O}}_2^0 = 3L_z^2 - L(L+1)$)

https://doi.org/10.1021/acs.inorgchem.4c01672
Inorg. Chem. 2024, 63, 17198−17207

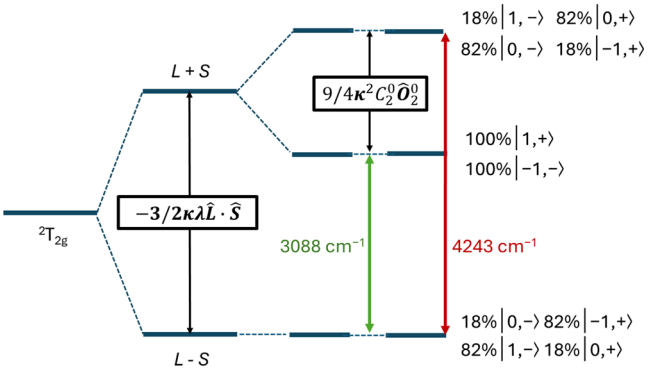

Figure 5. Schematic representation of the electronic energy structure of $[Os(acac)_3]$ as obtained by the analysis of EPR and magnetic measurements. The energy differences between the states are reported in green and red. On the right, composition of the states in the $|M_L\ M_S\rangle$ basis is reported.

and third and fourth terms describe the Zeeman effect on the spin and on the orbital angular momentum ($g_e = 2.0023$, $g_L = 1$) Finally, κ is the orbital-reduction factor, which takes into account the covalency, whereas $-3/2$ is a constant introduced by T−P isomorphism. The best simulation was obtained by fixing the spin orbit constant to $\lambda = -3100$ cm^{-1} and by adjusting the orbital reduction factor ($\kappa = 0.498 \pm 0.05$) and the axial second order crystal field parameter ($C_2^0 = -920$ cm^{-1}). The mean field was introduced as[12,82]

$$\chi = \frac{\chi}{1 - \chi\cdot(2zJ'/Ng^2\beta^2)} \quad (4)$$

The best obtained value was $zJ' = 0.39$ cm^{-1}, confirming the ferromagnetic nature of the intermolecular interactions.

Hamiltonian (3) with the best fit parameters obtained for rationalizing the dc magnetic data can be used to calculate the g values of the ground doublet. These are in excellent agreement ($g_{\parallel calc} = 2.50$, $g_{\perp\ calc} = 1.18$) with the ones obtained from EPR, emphasizing the robustness of the model.

Given the interest of largely anisotropic magnetic centers in the search for new SMM, the magnetization dynamics of $[Os(acac)_3]$ was studied by ac measurements. The compound did not show slow relaxation in zero applied field at the lowest temperature (2 K). When an external magnetic field was applied, a peak in the out-of-phase susceptibility appeared (Figure 6a). While for low fields (<0.5 T), the peak is too broad to be fitted, between 0.5 and 1.0 T, the curves could be fitted with a Debye model.[83] At higher fields the peak broadens again and moves toward lower frequencies. The relatively low value of χ' at low frequency (ca. 0.08 cm^3 mol^{-1}, Figure S10 in Supporting Information) compared to the χ obtained with the dc measurements (ca. 0.16 cm^3 mol^{-1}) suggests the presence of another relaxation process at lower frequency. The large values of the parameter accounting for the distribution of the relaxation times t (α parameter reported in Table S3 of the Supporting Information) indicate that the main active process is related to dipolar fields. Furthermore, t increases monotonously with the field (red symbols in Figure 6c) and no trace of contribution from a direct relaxation process (for which t would decrease as

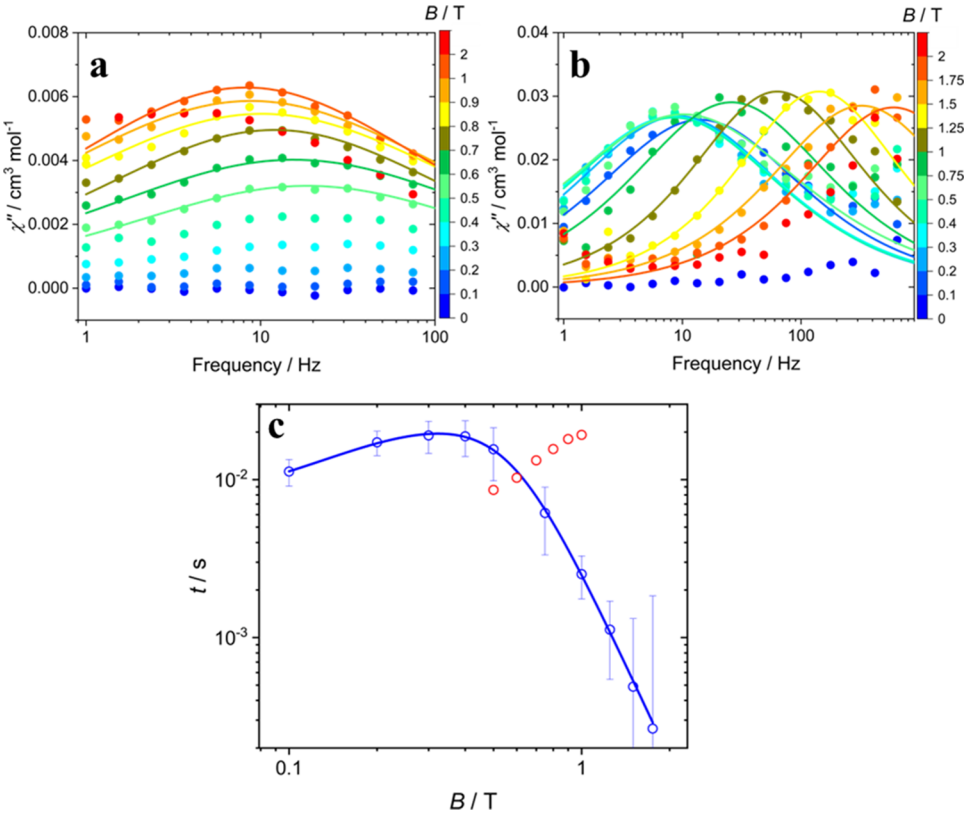

Figure 6. Frequency dependence of the imaginary component of susceptibility at 2 K from 0 to 2.0 T for pure (a) and diluted (b) $[Os(acac)_3]$. Relaxation at higher frequency region did not give appreciable signal. (c) Relaxation time of β (red) and diluted (blue) $[Os(acac)_3]$. The continuous line represents the best fit obtained with the parameters reported in the text.

https://doi.org/10.1021/acs.inorgchem.4c01672
Inorg. Chem. 2024, 63, 17198−17207

B^{-n}, $n = 2$ or 4)[84] could be detected. To reduce the effect of the dipolar fields on the relaxation dynamics, we measured the same Ga-diluted compound investigated using EPR measurements. The application of an external field causes the appearance of peaks in χ'' at lower frequencies compared to the pure $[Os(acac)_3]$, demonstrating that magnetic dilution is effective in slowing down the relaxation (Figures 6b and S10 in Supporting Information). As expected, the α values (Table S4 of the Supporting Information) are now significantly lower than in the pure complex. The fitted relaxation time does not monotonously vary with the field (blue symbols in Figure 6c), in close resemblance with other $S = 1/2$ systems, suggesting a competition between a direct process and a field-dependent Raman process.[4] Therefore, we have fitted the experimental data using the Brons-van Vleck equation:

$$t^{-1} = c\mathbf{B}^4 + d\frac{1 + e\mathbf{B}^2}{1 + f\mathbf{B}^2} \quad (5)$$

where the first term describes the field-dependence of the direct mechanism, and the second term takes into account the effect of the internal magnetic field in promoting Raman relaxation. The best fit values obtained from the fit are $c = 363(17)\ s^{-1}\cdot T^{-4}$, $d = 141(17)\ s^{-1}$, $f = 106(32)\ T^{-2}$ and $e = 29(6)\ T^{-2}$.

Slowly relaxing complexes where the magnetization dynamics stems from the Osmium center are exceedingly rare in the literature; therefore, a meaningful comparison between measured relaxation times is somewhat difficult. Recently, Su et al. reported a study on osmium(V) and osmium(III) complexes.[80] While their osmium(III) complex did not show any slow relaxation, the osmium(V) complex showed an in-field relaxation with a relaxation time at $T = 2$ K ca. 2 orders of magnitude faster than the one reported here for Os@$[Ga(acac)_3]$.

4. CONCLUSIONS

In this study, we reported a detailed magnetic study on a polymorph of the $[Os(acac)_3]$ metal complex. In the absence of a clear X-ray structural resolution, the combination of EPR and CTM (never used on an osmium complex) was used to prove that the studied system belongs to the orthorhombic space group, therefore demonstrating full isomorphism along the group 8 of the periodic table. This is the first dimorphic acetylacetonate complex of a 5d metal. Our study evidenced a pronounced uniaxial magnetic anisotropy of the ground doublet, enforced by the structural rigidity of the bidentate ligands, with the easy axis pointing along the pseudo-C_3 axis of the molecule. Notably, we also reported the first hyperfine splitting of an osmium complex. A magnetometric analysis evidenced the presence of a ferromagnetic mean field. The complex exhibited in-field slow relaxation of magnetization that could be further slowed by suppressing dipolar fields via magnetic dilution. Our work provides an excellent rationalization of the electronic structure of a 5d complex, which was absent in the recent literature, and we believe that this can be a trigger for developing new systems where the properties of heavy metals can be exploited.

■ ASSOCIATED CONTENT

Supporting Information

The Supporting Information is available free of charge at https://pubs.acs.org/doi/10.1021/acs.inorgchem.4c01672.

Structural analysis (PXRD, cell analysis), crystal pictures, magnetic anisotropy main axes, supplementary ac measurements, best fit parameters, visual representation of the torque rotations, and MATLAB codes (PDF)

■ AUTHOR INFORMATION

Corresponding Author

Mauro Perfetti − *Department of Chemistry "Ugo Schiff", DICUS and INSTM Research Unit, University of Florence, 50019 Sesto Fiorentino, Florence, Italy;* orcid.org/0000-0001-5649-0449; Email: mauro.perfetti@unifi.it

Authors

Arsen Raza − *Department of Chemistry "Ugo Schiff", DICUS and INSTM Research Unit, University of Florence, 50019 Sesto Fiorentino, Florence, Italy; Department of Industrial Engineering, DIEF and INSTM Research Unit, University of Florence, 50139 Florence, Italy*

Laura Chelazzi − *Centro di Servizi di Cristallografia Strutturale, CRIST, 50019 Sesto Fiorentino, Florence, Italy*

Samuele Ciattini − *Centro di Servizi di Cristallografia Strutturale, CRIST, 50019 Sesto Fiorentino, Florence, Italy*

Lorenzo Sorace − *Department of Chemistry "Ugo Schiff", DICUS and INSTM Research Unit, University of Florence, 50019 Sesto Fiorentino, Florence, Italy;* orcid.org/0000-0003-4785-1331

Complete contact information is available at: https://pubs.acs.org/10.1021/acs.inorgchem.4c01672

Author Contributions

A.R. synthesized the complexes and performed the chemical characterization. S.C. and L.C. performed some of the crystallographic measurements and analysis, together with A.R. A.R. and L.S. performed the EPR measurements and modeling. A.R. and M.P. performed the magnetic measurements and the modeling. All authors contributed in writing the paper.

Notes

The authors declare no competing financial interest.

■ ACKNOWLEDGMENTS

This work was funded by the European Union (ERC, ELECTRA, 101039890). Views and opinions expressed are however those of the authors only and do not necessarily reflect those of the European Union or the European Research Council. Neither the European Union nor the granting authority can be held responsible for them. The financial support provided by the MUR - Dipartimenti di Eccellenza 2023-2027 (DICUS 2.0) (ref no. B96C1700020008) to the Department of Chemistry "Ugo Schiff" of the University of Florence is acknowledged.

■ REFERENCES

(1) Raza, A.; Perfetti, M. Electronic structure and magnetic anisotropy design of functional metal complexes. *Coord. Chem. Rev.* **2023**, *490*, No. 215213.

(2) Fataftah, M. S.; Zadrozny, J. M.; Coste, S. C.; Graham, M. J.; Rogers, D. M.; Freedman, D. E. Employing Forbidden Transitions as Qubits in a Nuclear Spin-Free Chromium Complex. *J. Am. Chem. Soc.* **2016**, *138* (4), 1344−1348.

(3) Atzori, M.; Tesi, L.; Morra, E.; Chiesa, M.; Sorace, L.; Sessoli, R. Room-Temperature Quantum Coherence and Rabi Oscillations in Vanadyl Phthalocyanine: Toward Multifunctional Molecular Spin Qubits. *J. Am. Chem. Soc.* **2016**, *138* (7), 2154−2157.

(4) Tesi, L.; Lucaccini, E.; Cimatti, I.; Perfetti, M.; Mannini, M.; Atzori, M.; Morra, E.; Chiesa, M.; Caneschi, A.; Sorace, L.; Sessoli, R. Quantum coherence in a processable vanadyl complex: new tools for the search of molecular spin qubits. *Chem. Sci.* **2016**, *7* (3), 2074−2083.
(5) Warner, M.; Din, S.; Tupitsyn, I. S.; Morley, G. W.; Stoneham, A. M.; Gardener, J. A.; Wu, Z.; Fisher, A. J.; Heutz, S.; Kay, C. W.; Aeppli, G. Potential for spin-based information processing in a thin-film molecular semiconductor. *Nature* **2013**, *503* (7477), 504−508.
(6) Bader, K.; Dengler, D.; Lenz, S.; Endeward, B.; Jiang, S. D.; Neugebauer, P.; van Slageren, J. Room temperature quantum coherence in a potential molecular qubit. *Nat. Commun.* **2014**, *5*, 5304.
(7) Pedersen, K. S.; Schau-Magnussen, M.; Bendix, J.; Weihe, H.; Palii, A. V.; Klokishner, S. I.; Ostrovsky, S.; Reu, O. S.; Mutka, H.; Tregenna-Piggott, P. L. Enhancing the blocking temperature in single-molecule magnets by incorporating 3d-5d exchange interactions. *Chem.—Eur. J.* **2010**, *16* (45), 13458−13464.
(8) Pedersen, K. S.; Woodruff, D. N.; Singh, S. K.; Tressaud, A.; Durand, E.; Atanasov, M.; Perlepe, P.; Ollefs, K.; Wilhelm, F.; Mathoniere, C.; Neese, F.; Rogalev, A.; Bendix, J.; Clerac, R. [OsF(6)](x-): Molecular Models for Spin-Orbit Entangled Phenomena. *Chem.—Eur. J.* **2017**, *23* (47), 11244−11248.
(9) Pedersen, K. S.; Bendix, J.; Tressaud, A.; Durand, E.; Weihe, H.; Salman, Z.; Morsing, T. J.; Woodruff, D. N.; Lan, Y.; Wernsdorfer, W.; Mathoniere, C.; Piligkos, S.; Klokishner, S. I.; Ostrovsky, S.; Ollefs, K.; Wilhelm, F.; Rogalev, A.; Clerac, R. Iridates from the molecular side. *Nat. Commun.* **2016**, *7*, 12195.
(10) Dreiser, J.; Pedersen, K. S.; Schnegg, A.; Holldack, K.; Nehrkorn, J.; Sigrist, M.; Tregenna-Piggott, P.; Mutka, H.; Weihe, H.; Mironov, V. S.; Bendix, J.; Waldmann, O. Three-axis anisotropic exchange coupling in the single-molecule magnets NEt4[Mn(III)2(5-Brsalen)2(MeOH)-2M(III)(CN)6] (M = Ru, Os). *Chem.—Eur. J.* **2013**, *19* (11), 3693−3701.
(11) Pedersen, K. S.; Sørensen, M. A.; Bendix, J. Fluoride-coordination chemistry in molecular and low-dimensional magnetism. *Coord. Chem. Rev.* **2015**, *299*, 1−21.
(12) Pinkowicz, D.; Southerland, H. I.; Avendano, C.; Prosvirin, A.; Sanders, C.; Wernsdorfer, W.; Pedersen, K. S.; Dreiser, J.; Clerac, R.; Nehrkorn, J.; Simeoni, G. G.; Schnegg, A.; Holldack, K.; Dunbar, K. R. Cyanide Single-Molecule Magnets Exhibiting Solvent Dependent Reversible "On" and "Off" Exchange Bias Behavior. *J. Am. Chem. Soc.* **2015**, *137* (45), 14406−14422.
(13) Guo, J. F.; Yeung, W. F.; Lau, P. H.; Wang, X. T.; Gao, S.; Wong, W. T.; Chui, S. S.; Che, C. M.; Wong, W. Y.; Lau, T. C. trans-[Os(III)(salen)(CN)(2)](−): a new paramagnetic building block for the construction of molecule-based magnetic materials. *Inorg. Chem.* **2010**, *49* (4), 1607−1614.
(14) Groom, C. R.; Bruno, I. J.; Lightfoot, M. P.; Ward, S. C. The Cambridge Structural Database. *Acta Crystallogr., Sect. B: Struct. Sci.* **2016**, *72* (Pt 2), 171−179.
(15) Astbury, W. T. The structure and isotrimorphism of the tervalent metallic acetylacetones. *Proc. R. Soc. London, Ser. A* **1926**, *112* (761), 448−467.
(16) Arslan, E.; Lalancette, R. A.; Bernal, I. An historic and scientific study of the properties of metal(III) tris-acetylacetonates. *Struct. Chem.* **2017**, *28* (1), 201−212.
(17) Sodhi, R. K.; Paul, S. An Overview of Metal Acetylacetonates: Developing Areas/Routes to New Materials and Applications in Organic Syntheses. *Catal. Surv. Asia* **2018**, *22* (1), 31−62.
(18) National Academy of Sciences; Nuclear Science Series. *The Radiochemistry of Uranium*; The National Academies Press: Washington, DC, 1962; p 358.
(19) Fahlman, B. D.; Barron, A. R. Substituent effects on the volatility of metal β-diketonates. *Adv. Mater. Opt. Electron.* **2000**, *10* (3−5), 223−232.
(20) Siddiqi, M. A.; Siddiqui, R. A.; Atakan, B. Thermal stability, sublimation pressures and diffusion coefficients of some metal acetylacetonates. *Surf. Coat. Technol.* **2007**, *201* (22−23), 9055−9059.
(21) Pinna, N.; Garnweitner, G.; Antonietti, M.; Niederberger, M. A general nonaqueous route to binary metal oxide nanocrystals involving a C-C bond cleavage. *J. Am. Chem. Soc.* **2005**, *127* (15), 5608−5612.
(22) Wagh, Y. S.; Bhanage, B. M. Cu(acac)2 catalyzed oxidative C−H bond amination of azoles with amines under base-free conditions. *Tetrahedron Lett.* **2012**, *53* (48), 6500−6503.
(23) Pastusiak, M.; Dobrzynski, P.; Kasperczyk, J.; Smola, A.; Janeczek, H.Synthesis of biodegradable high molecular weight polycarbonates from 1,3-trimethylene carbonate and 2,2-dimethyltrimethylene carbonate. *J. Appl. Polym. Sci.* **2013**, *131*, 5 .
(24) Kalyanam, N.; Gandhi, V. G.; Sivaram, S. Acrylonitrile copolymers using cobalt acetylacetonate-triethylaluminum initiator system. *Polym. Bull.* **1984**, *11* (2), 105−108.
(25) Belykh, L. B.; Goremyka, T. V.; Belonogova, L. N.; Schmidt, F. K. Highly active and selective catalysts of hydrogenation based on palladium bis-acetylacetonate and phenylphosphine. *J. Mol. Catal. A Chem.* **2005**, *231* (1−2), 53−59.
(26) Consorti, C. S.; Umpierre, A. P.; Souza, R. F. D.; Dupont, J.; Suarez, P. A. Z. Selective hydrogenation of 1,3-butadiene by transition metal compounds immobilized in 1-butyl-3-methyl imidazolium room temperature ionic liquids. *J. Braz. Chem. Soc.* **2003**, *14* (3), 401−405.
(27) Mata, Y.; Dieguez, M.; Pamies, O.; Woodward, S. Screening of a modular sugar-based phosphite ligand library in the asymmetric nickel-catalyzed trialkylaluminum addition to aldehydes. *J. Org. Chem.* **2006**, *71* (21), 8159−8165.
(28) Xiao, X.; Wang, H.; Huang, Z.; Yang, J.; Bian, X.; Qin, Y. Selective diethylzinc reduction of imines in the presence of ketones catalyzed by Ni(acac)2. *Org. Lett.* **2006**, *8* (1), 139−142.
(29) Hara, Y.; Kusaka, H.; Inagaki, H.; Takahashi, K.; Wada, K. A Novel Production of γ-Butyrolactone Catalyzed by Ruthenium Complexes. *J. Catal.* **2000**, *194* (2), 188−197.
(30) Cotton, F. A.; Rice, C. E.; Rice, G. W. The crystal and molecular structures of bis(2,4-pentanedionato)chromium. *Inorg. Chim. Acta* **1977**, *24*, 231−234.
(31) Starikova, Z. A.; Shugam, E. A. Crystal chemical data for inner complexes of β-diketones. *J. Struct. Chem.* **1969**, *10* (2), 267−269.
(32) Anderson, T. J.; Neuman, M. A.; Melson, G. A. Coordination chemistry of scandium. V. Crystal and molecular structure of tris (acetylacetonato)scandium(III). *Inorg. Chem.* **1973**, *12* (4), 927−930.
(33) McGarvey, B. R. Electron Spin Resonance of Titanium (III) Acetylacetonate. *J. Chem. Phys.* **1963**, *38* (2), 388−392.
(34) McGarvey, B. R. Anisotropic Hyperfine Interaction of Cr53 in Chromium (III) Acetylacetonate. *J. Chem. Phys.* **1964**, *40* (3), 809−812.
(35) Krzystek, J.; Yeagle, G. J.; Park, J. H.; Britt, R. D.; Meisel, M. W.; Brunel, L. C.; Telser, J. High-frequency and -field EPR spectroscopy of tris(2,4-pentanedionato)manganese(III): investigation of solid-state versus solution Jahn-Teller effects. *Inorg. Chem.* **2003**, *42* (15), 4610−4618.
(36) Krzystek, J.; Yeagle, G. J.; Park, J.-H.; Britt, R. D.; Meisel, M. W.; Brunel, L.-C.; Telser, J. High-Frequency and -Field EPR Spectroscopy of Tris(2,4-pentane-dionato)manganese(III): Investigation of Solid-State Versus Solution Jahn−Teller Effects. *Inorg. Chem.* **2006**, *45* (24), 9926−9926.
(37) Krzystek, J.; Yeagle, G. J.; Park, J.-H.; Britt, R. D.; Meisel, M. W.; Brunel, L.-C.; Telser, J. High-Frequency and -Field EPR Spectroscopy of Tris(2,4-pentanedionato)manganese(III): Investigation of Solid-State versus Solution Jahn−Teller Effects. *Inorg. Chem.* **2009**, *48* (7), 3290−3290.
(38) Ledneva, A. Y.; Artemkina, S. B.; Piryazev, D. A.; Fedorov, V. E. Structure and thermal properties of the molybdenum complex Mo(acac)3. *J. Struct. Chem.* **2015**, *56* (5), 1021−1023.
(39) Hashimoto, K.; Kabuto, C.; Omori, T.; Yoshihara, K. Molecular Structure of Tris(acetylacetonato)technetium(III). *Chem. Lett.* **1988**, *17* (8), 1379−1380.
(40) Dallmann, K.; Preetz, W. Darstellung, Kristallstruktur, Schwingungsspektren und Normalkoordinatenanalyse von [Os(acac)-3]/ Synthesis, Crystal Structure, Vibrational Spectra, and Normal

https://doi.org/10.1021/acs.inorgchem.4c01672
Inorg. Chem. 2024, 63, 17198−17207

Coordinate Analysis of [Os(acac)3]. *Z. Naturforsch. B* **1998**, *53* (2), 232−238.
(41) Davignon, L.; Dereigne, A.; Manoli, J. M.; Davous, P. Étude cristallographique du tris (pentanedione-2,4) iridium(III), du tris (trifluoro-1,1,1 pentanedione-2,4) rhodium(III) et du tris (trifluoro-1,1,1 pentanedione-2,4) iridium(III). *J. Less Common Met.* **1970**, *21* (3), 345−351.
(42) Ha, K. Crystal structure of bis(pentane-2,4-dionato-) k2O,O')-platinum(II), Pt(C5H7O2)2. *New Crystal Structures* **2014**, *226*, 329−330.
(43) Allard, B. Studies of tetravalent acetylacetonato complexes—I: Coordination and properties in the solid state. *Journal of Inorganic and Nuclear Chemistry* **1976**, *38*, 2109−2115.
(44) Yun, S. S.; Suh, I.-H.; Choi, S.-S.; Kim, T.-H.; Lee, S. Alternative Formation and Crystal Structure of Tris(Acetylacetonato)Titanium-(Hi) from Titanocene and 2, 4-Pentanedione. *J. Coord. Chem.* **1999**, *47* (2), 315−318.
(45) Morosin, B.; Montgomery, H. The crystal structure of α- and β-tris(2,4-pentanedionato)vanadium(III). *Acta Crystallogr. B* **1969**, *25* (7), 1354−1359.
(46) Kavitha, S. J.; Panchanatheswaran, K.; Low, J. N.; Glidewell, C. The α polymorph of racemic tris(2,4-pentanedionato-κ2O,O′)-vanadium(III), redetermined at 120 K. *Acta Crystallogr. E* **2005**, *61* (7), m1326−m1328.
(47) Sokolov, M. N.; Virovets, A. V.; Rogachev, A. V.; Abramov, P. A.; Fedin, V. P. Interaction of [VO(OPr)3] with hexamethyldisilthiane in the presence of β-diketones. *Coordination chemistry* **2013**, *39* (2), 86−91.
(48) Morosin, B.; Brathovde, J. R. The crystal structure and molecular configuration of trisacetylacetonatomanganese(III). *Acta Crystallogr.* **1964**, *17* (6), 705−711.
(49) Stults, B. R.; Marianelli, R. S.; Day, V. W. Distortions of the coordination polyhedron in high-spin manganese(III) complexes. 3. Crystal and molecular structure of.gamma.-tris(acetylacetonato)-manganese(III): a tetragonally elongated octahedral form. *Inorg. Chem.* **1979**, *18* (7), 1853−1858.
(50) Baker, T. M.; Howard, K. M.; Brennessel, W. W.; Neidig, M. L. Crystal structure of a third polymorph of tris-(acetyl-acetonato-kappa(2) O,O')iron(III). *Acta Crystallogr., Sect. E: Crystallogr. Commun.* **2015**, *71* (Pt 12), m228−m229.
(51) Chao, G. K. J.; Sime, R. L.; Sime, R. J. The crystal and molecular structure of tris-acetylacetonatoruthenium(III). *Acta Crystallogr. B* **1973**, *29* (12), 2845−2849.
(52) Knowles, T. S.; Howlin, B. J.; Jones, J. R.; Povey, D. C.; Amodio, C. A. Structures of α-tris (2,4-pentanedionato) ruthenium(III) and tris(3-bromo-2,4-pentanedionato) ruthenium(III). *Polyhedron* **1993**, *12* (24), 2921−2924.
(53) Wakisaka, T.; Kusada, K.; Yamamoto, T.; Toriyama, T.; Matsumura, S.; Ibrahima, G.; Seo, O.; Kim, J.; Hiroi, S.; Sakata, O.; Kawaguchi, S.; Kubota, Y.; Kitagawa, H. Discovery of face-centred cubic Os nanoparticles. *Chem. Commun.* **2020**, *56* (3), 372−374.
(54) Wang, X. Y.; Avendano, C.; Dunbar, K. R. Molecular magnetic materials based on 4d and 5d transition metals. *Chem. Soc. Rev.* **2011**, *40* (6), 3213−3238.
(55) Fiechter, M. R.; Haase, P. A. B.; Saleh, N.; Soulard, P.; Tremblay, B.; Havenith, R. W. A.; Timmermans, R. G. E.; Schwerdtfeger, P.; Crassous, J.; Darquie, B.; Pasteka, L. F.; Borschevsky, A. Toward Detection of the Molecular Parity Violation in Chiral Ru(acac)(3) and Os(acac)(3). *J. Phys. Chem. Lett.* **2022**, *13* (42), 10011−10017.
(56) Sheldrick, G. M. Crystal structure refinement with SHELXL. *Acta Crystallogr., Sect. C: Struct. Chem.* **2015**, *71* (Pt 1), 3−8.
(57) Farrugia, L. J. WinGXandORTEP for Windows: an update. *J. Appl. Crystallogr.* **2012**, *45* (4), 849−854.
(58) Bain, G. A.; Berry, J. F. Diamagnetic corrections and Pascal's constants. *J. Chem. Educ.* **2008**, *85* (4), 532.
(59) Stoll, S.; Schweiger, A. EasySpin, a comprehensive software package for spectral simulation and analysis in EPR. *J. Magn. Reson.* **2006**, *178* (1), 42−55.
(60) Pellegrino, A. L.; Mezzalira, C.; Mazzer, F.; Cadi Tazi, L.; Caneschi, A.; Gatteschi, D.; Fragalà, I. L.; Speghini, A.; Sorace, L.; Malandrino, G. Multifunctional "Dy(hfa)3●glyme" adducts: Synthesis and magnetic/luminescent behaviour. *Inorg. Chim. Acta* **2022**, *535*, 120851.
(61) Dwyer, F. P.; Sargeson, A. Tris-acetylacetone-osmium(III). *J. Am. Chem. Soc.* **1955**, *77* (5), 1285−1285.
(62) Harris, K. D. M.; Tremayne, M.; Kariuki, B. M. Contemporary Advances in the Use of Powder X-Ray Diffraction for Structure Determination. *Angew. Chem., Int. Ed.* **2001**, *40* (9), 1626−1651.
(63) Giacovazzo, C.; Monaco, H. L.; Viterbo, D.; Scordari, F.; Gilli, G.; Zanotti, G.; Catti, M. *Fundamentals of crystallography*; Oxford University Press, 1992.
(64) Pawley, G. S. Unit-cell refinement from powder diffraction scans. *J. Appl. Crystallogr.* **1981**, *14* (6), 357−361.
(65) AXS, B. *TOPASv6*, 2016.
(66) Medina, A. N.; Gandra, F. G.; Baesso, M. L.; Lima, J. B.; McGarvey, B. R.; Franco, D. W. Determination of electron paramagnetic resonance parameters for osmium(III) low-spin systems using graphical solutions. *J. Chem. Soc., Faraday Trans.* **1997**, *93* (11), 2105−2111.
(67) DeSimone, R. E. Electron paramagnetic resonance studies of low-spin d5 complexes. Trisbidentate complexes of iron(III), ruthenium-(III), and osmium(III) with sulfur-donor ligands. *J. Am. Chem. Soc.* **1973**, *95* (19), 6238−6244.
(68) McGarvey, B. R. Survey of ligand field parameters of strong field d5 complexes obtained from the g matrix. *Coord. Chem. Rev.* **1998**, *170* (1), 75−92.
(69) Rieger, P. H. Electron paramagnetic resonance studies of low-spin d5 transition metal complexes. *Coord. Chem. Rev.* **1994**, *135−136*, 203−286.
(70) Chicco, S.; Chiesa, A.; Allodi, G.; Garlatti, E.; Atzori, M.; Sorace, L.; De Renzi, R.; Sessoli, R.; Carretta, S. Controlled coherent dynamics of [VO(TPP)], a prototype molecular nuclear qudit with an electronic ancilla. *Chem. Sci.* **2021**, *12* (36), 12046−12055.
(71) DeSimone, R. E.; Drago, R. S. Magnetic resonance studies of some low-spin d5 tris diimine complexes. *J. Am. Chem. Soc.* **1970**, *92* (8), 2343−2352.
(72) Singer, L. S. Paramagnetic Resonance Absorption in Some Cr+3 Complexes. *J. Chem. Phys.* **1955**, *23* (2), 379−388.
(73) Figgis, B. N.; Reynolds, P. A.; Murray, K. S.; Moubaraki, B. The Ground State in Tris(acetylacetonato)ruthenium(III) from Low-Temperature Single-Crystal Magnetic Properties. *Aust. J. Chem.* **1998**, *51* (3), 229−234.
(74) Albores, P.; Slep, L. D.; Baraldo, L. M.; Baggio, R.; Garland, M. T.; Rentschler, E. Crystal structure and electronic and magnetic properties of hexacyanoosmate(III). *Inorg. Chem.* **2006**, *45* (6), 2361−2363.
(75) Perfetti, M.; Serri, M.; Poggini, L.; Mannini, M.; Rovai, D.; Sainctavit, P.; Heutz, S.; Sessoli, R. Molecular Order in Buried Layers of TbPc2 Single-Molecule Magnets Detected by Torque Magnetometry. *Adv. Mater.* **2016**, *28* (32), 6946−6951.
(76) Perfetti, M. Cantilever torque magnetometry on coordination compounds: from theory to experiments. *Coord. Chem. Rev.* **2017**, *348*, 171−186.
(77) Rigamonti, L.; Cornia, A.; Nava, A.; Perfetti, M.; Boulon, M. E.; Barra, A. L.; Zhong, X.; Park, K.; Sessoli, R. Mapping of single-site magnetic anisotropy tensors in weakly coupled spin clusters by torque magnetometry. *Phys. Chem. Chem. Phys.* **2014**, *16* (32), 17220−17230.
(78) Rigamonti, L.; Cotton, C.; Nava, A.; Lang, H.; Ruffer, T.; Perfetti, M.; Sorace, L.; Barra, A. L.; Lan, Y.; Wernsdorfer, W.; Sessoli, R.; Cornia, A. Diamondoid Structure in a Metal-Organic Framework of Fe4 Single-Molecule Magnets. *Chem.—Eur. J.* **2016**, *22* (38), 13705−13714.
(79) Lucaccini, E.; Briganti, M.; Perfetti, M.; Vendier, L.; Costes, J. P.; Totti, F.; Sessoli, R.; Sorace, L. Relaxation Dynamics and Magnetic Anisotropy in a Low-Symmetry Dy(III) Complex. *Chem.—Eur. J.* **2016**, *22* (16), 5552−5562.

https://doi.org/10.1021/acs.inorgchem.4c01672
Inorg. Chem. 2024, 63, 17198−17207

(80) Su, Q. Q.; Fan, K.; Huang, X. D.; Xiang, J.; Cheng, S. C.; Ko, C. C.; Zheng, L. M.; Kurmoo, M.; Lau, T. C. Field-induced slow magnetic relaxation in low-spin S = 1/2 mononuclear osmium(v) complexes. *Dalton Trans.* **2020**, *49* (13), 4084−4092.
(81) Griffith, J. S. *The Theory of Transition-metal Ions*; Cambridge University Press, 1961.
(82) O'Connor, C. J. Magnetochemistry—Advances in Theory and Experimentation. *Prog. Inorg. Chem.* **1982**, *29*, 203−283.
(83) Gatteschi, D.; Sessoli, R.; Villain, J. *Molecular Nanomagnets*; OUP Oxford, 2011.
(84) Orbach, R. Spin-lattice relaxation in rare-earth salts. *Proc. R. Soc. London, Ser. A* **1961**, *264* (1319), 458−484.

https://doi.org/10.1021/acs.inorgchem.4c01672
Inorg. Chem. 2024, 63, 17198−17207